Use of dynamical information in a four-dimensional variational assimilation

Jean-Noël Thépaut* Philippe Courtier* Ross N. Hoffman**

* European Centre for Medium-range Weather Forecasts, Reading, UK.
** Atmospheric and Environmental Research, Inc., Cambridge, MA, USA.

Abstract

A four-dimensional (4d) variational assimilation (4dVAR) seeks an optimal balance between observations scattered in time and space over a finite 4d analysis volume and *a priori* information. In some cases, 4dVAR is able to closely fit both observations and the *a priori* initial estimate, by making very small changes to the initial conditions which correspond to those rapidly growing perturbations which have large amplitude at the observation locations and times. Some observations may occur at locations and times for which the amplitudes of rapidly growing perturbations are not large. In order to fit such data larger changes to the initial conditions are necessary. Such cases may result in amplification of the analysis increments away from the observation locations. This situation occurs generally for surface data, because of the damping effect of surface exchange processes. These interactions are seen in experiments using single observations.

To further explore the impact of surface data in 4dVAR, we conduct experiments with and without ERS1 *C* band measurements of backscatter. As expected and in contrast to conventional approaches, the impact is not confined to the lower troposphere and the analysis increments are balanced. We focus on the case of a small intense North Atlantic storm which struck the coast of Norway on New Year's Day, 1992. The scatterometer data do have a significant, apparently positive, impact on the 4dVAR analysis in this case. The example using scatterometer data also demonstrates the ease with which 4dVAR assimilates nonstandard data, which have a complex, highly nonlinear relationship with the model variables.

1 Introduction.

A four-dimensional (4d) variational assimilation (4dVAR) seeks an optimal balance between observations scattered in time and space over a finite 4d analysis volume and *a priori* information (Thépaut and Courtier, 1991; Rabier and Courtier, 1992; Thépaut et al., 1993). The key *a priori* information used in 4dVAR is knowledge of the dynamics of the atmosphere. In addition 4dVAR ordinarily uses an estimate of the initial conditions, i.e., the atmospheric state at the start of the analysis period. (This background information is used in the experiments described here.) Because the atmospheric dynamics allow for extremely rapid growth of small initial perturbations, it is possible to fit observations at the end of the analysis period by making very small changes to the initial conditions. In certain experiments with a single observation at the end of the analysis period (Section 3.1), we will show a strong correlation between the analysis increments, i.e. the analysis minus the initial estimate, and the most rapidly growing linear perturbations, for the given atmospheric state and for the time period of the analysis.

Thus in some cases, the 4dVAR is able to closely fit both observations and the *a priori* initial estimate, by making very small changes to the initial conditions which correspond to those rapidly growing perturbations which have large amplitude at the observation locations and times. Of course observations may in principle occur anywhere and at various times. A large observation increment near the start of the analysis period will necessarily require a large change to the initial conditions. Similarly, observations at later times may occur at locations (e.g. in the boundary layer) for which the amplitudes of rapidly growing perturbations are not large. Again larger changes to the initial conditions will be necessary. In some of these cases, a very rapidly growing perturbation may still be the most "economical" way of fitting the data. In such a case the amplitude of this perturbation will be large, but not maximal at the observation location, and the analysis increments will be largest not at the observation location, but at the location of the maximum amplitude of the growing perturbation. This situation occurs generally for surface data, because of the damping effect of surface exchange processes.

We will demonstrate this amplification of the analysis increments away from the observation locations in the case of a single surface wind observation (Section 3.2). This experiment shows that the impact of surface observations will be very different in 4dVAR from the impact seen in static analyses either from the standard so-called "optimum interpolation" (OI) analysis or the 3d variational analysis (3dVAR). In particular in static analyses, the impact of surface data on the analysis tends to decay with height, whereas in certain 4dVAR analyses this impact grows with height. Furthermore, during subsequent forecasts, we expect analysis increments confined to the surface to damp out due to surface friction. Additionally, in 4dVAR the influence of the data is extended in the horizontal to greater distances and in nonisotropic patterns. The 4dVAR response to a single observation at the end of the analysis period is proportional to covariances predicted by the Kalman filter for this problem. Our results therefore serve to demonstrate the potential three-dimensional complexity of such covariances, already shown explicitly by Gauthier et al. (1993) for the extended Kalman filter in the case of non-linear barotropic dynamics.

To further explore the impact of surface data in 4dVAR, we examine the impact of

ERS1 C band measurements of backscatter (Section 4). These scatterometer measurements are closely, but highly nonlinearly, related to marine surface winds. As expected and in contrast to conventional approaches, the impact is not confined to the surface and the analysis increments are balanced. We focus on the case of a small intense North Atlantic storm which struck the coast of Norway on New Year's Day, 1992. The scatterometer data do have a significant impact on the 4dVAR in this case. Evidence from the high resolution operational analysis and forecast and from AVHRR imagery lead us to conclude that this impact is positive.

The example using scatterometer data also demonstrates the ease with which 4dVAR assimilates nonstandard data, which have a complex, highly nonlinear relationship with the model variables. The scatterometer data are notorious for having a directional ambiguity (Price, 1976). Generally 2 or 4 distinct wind vectors or ambiguities may be determined from the backscatter measurements at a single location. If the ambiguities can be ranked, and if the ambiguity ranked first does in fact have a high probability ($Pr > 0.6$) of being the closest ambiguity to the true wind, then spatial filtering techniques are effective at choosing the correct ambiguity (Schultz, 1991). Otherwise additional information must be used to resolve the ambiguities. This is the case for the ERS1 scatterometer. The variational assimilation method provides a natural means of combining the backscatter measurement with various other observations and *a priori* sources of information (Section 4).

2 Methodology.

In the experiments presented here, the 4dVAR assimilation determines the model evolution which minimizes a cost function. This cost function measures the sum of the misfits to the observations and to an estimate of the initial conditions at the start of the analysis period. The model is assumed to have no errors. By this expedient, the control variable, i.e. the variable which we vary to minimize the functional, is reduced to the initial conditions. However, the assumption of a perfect model, as well as fundamental predictability properties of the atmosphere (Gauthier, 1992), restrict the 4dVAR to limited time periods. Here all experiments are 24 hours in length.

In what follows we briefly present the functional, the model and the minimization procedures. The references cited below contain further details. Features of the 4dVAR which have not been formally published yet—the parametrization of vertical diffusion and surface friction, and the observations cost function for scatterometer σ^0 data—are presented in greater detail. Also we briefly present (again providing references) some results on the equivalence of 4dVAR and the Kalman filter, and on finite time optimal modes. These results are used below (Section 3) to explain the numerical results of the single observation experiments performed.

2.1 The 4dVAR cost function.

The principle of 4dVAR is to find a model solution which is as close as possible, in a least-square sense, to the observations available over a time period $[t_0, t_n]$. (The reader

is referred to Lorenc (1986) for a full presentation of the material of this section and of Section 2.6.) The solution may also be required to simultaneously satisfy other constraints either exactly or approximately. The misfit to the data and other approximate constraints is measured by a cost function. The smaller the cost function, the better the fit. For the case of Gaussian errors, a squared error cost function of the form given below should be used (Lorenc, 1986). In the present case an approximate constraint is based on a background, x_b. This background is an *a priori* estimate of x_0, the model state at the initial time t_0. If there are exact constraints, these are used to reduce the dimensionality of the control variable. In the present case the model dynamics are an exact constraint and the control variable is thereby reduced to x_0. These considerations lead to defining $J(x_0)$, the cost function for 4dVAR by,

$$J(x_0) = \frac{1}{2}(H(x_0) - y)^T O^{-1}(H(x_0) - y) + \frac{1}{2}(x_0 - x_b)^T B^{-1}(x_0 - x_b) \qquad (1)$$

Here y is the vector of observations distributed in time and space, H is the operator which predicts the observations from the model initial state, O is the covariance matrix of the observation and representativeness errors and B is the covariance matrix of the background errors. In practice the first term on the right hand side of (1) is broken up into a sum of smaller terms for different times and different observing systems by assuming the errors at different times and for different observing systems are uncorrelated. Note that (1) is also the cost function for 3dVAR if x_0 is replaced by x, the model state at the synoptic analysis time. For 3dVAR H provides the interpolation to the observation locations and the calculation of the observed variables. In 4dVAR H also includes the action of the forecast model.

2.2 The scatterometer observations cost function.

In Section 4 we present 4dVAR analyses with and without C band scatterometer data from the ERS1 satellite (Francis et al., 1991). Scatterometers are active radars which respond to the roughness of the ocean surface in the centimeter range principally via Bragg scattering. The measured physical quantity is radar backscatter, referred to as σ^0. Measurements of σ^0 show a strong dependence on wind speed and direction (Schroeder et al., 1982). In conventional scatterometer data processing, several collocated σ^0 measurements may be used to retrieve wind vectors (Jones et al., 1982). The retrieval is however ambiguous (Price, 1976). A further spatial filtering or reference to a background field is necessary (Schultz, 1991). To use the σ^0 data within 4dVAR we simply add a new observation cost function. In this way the 4dVAR approach combines the scatterometer wind retrieval and ambiguity removal problems with all other available information, including other types of observations and other constraints. The scatterometer cost function is

$$J_{scat} = \frac{1}{2}(H(x) - \sigma^0)^T O^{-1}(H(x) - \sigma^0) \qquad (2)$$

for each group of scatterometer data. Here x is the model state variable, at the time of the data (i.e., x is the forecast model state from initial conditions x_0) and H is composed of:

- An inverse spectral transform from spectral to grid-point space.
- A horizontal interpolation from the grid-points to the observation locations.
- A vertical interpolation to evaluate neutral stability wind at the reference height of the scatterometer (10 m) from wind at the lowest model level.
- A model function to compute the σ^0 that would be observed given the neutral stability wind.

The adjoint of all these operators is of course needed to compute the gradient of J_{scat} with respect to the control variable. In the present experiments the horizontal interpolation is linear in latitude and longitude. The vertical interpolation is based on a simple logarithmic wind profile with no stability correction. (However, provisions have been made to use the full boundary layer formulation in evaluating J_{scat}). In this case the 10 m neutral wind is a function of the lowest model layer wind, temperature and specific humidity, and the surface pressure and temperature.) The model function is the prelaunch CMOD2 (Long, 1991) as tuned by Stoffelen and Anderson (1992a). According to CMOD2, given the incidence angle, σ^0 depends only on the 10 m neutral wind speed and direction.

We assume that the scatterometer observational errors are uncorrelated. The observational standard deviation is usually given in terms of K_p , the expected standard deviation of σ^0 expressed as a fraction. That is the observational standard deviation is $K_p\sigma^0_{observed}$. K_p should account for several error sources, namely communication noise, radar equation and model function uncertainties and representativeness error. Large values of K_p generally occur for low wind speed, small incidence angles and small values of σ^0 . Here we use a model of K_p , polynomial in $\ln(\sigma^0)$ and incidence angle, developed for the model function and analysis resolution used. The calculated values of K_p range from 0.1 to 0.3. With these simplifications, J_{scat} takes the form

$$J_{scat} = \frac{1}{2}\sum_{\sigma^0}\frac{(\sigma^0_{model} - \sigma^0_{observed})^2}{(K_p\sigma^0_{observed})^2} \tag{3}$$

Both (2) and (3) are used for either 3dVAR or 4dVAR. Within the 3dVAR and 4dVAR configurations in the IFS system, the handling and use of the scatterometer σ^0 parallel in many respects the handling and use of TOVS radiance data (Pailleux et al., 1991 and Andersson et al., 1992).

2.3 The model and its adjoint.

The primitive equation model used in the following experiments is the IFS/ARPEGE code (cycle 9) which is described by Courtier et al. (1991). The vertical coordinate is the hybrid pressure-σ coordinate (Simmons and Burridge, 1981). The number of vertical levels is 19. Horizontally, spherical harmonics with a triangular truncation at degree 63, are used to represent vorticity, divergence, temperature, specific humidity and logarithm of surface pressure. The concatenation of these spherical harmonic coefficients for all vertical levels is the model state vector x. The number of points in the colocation grid in the vicinity

of the poles is reduced to save computing time (Hortal and Simmons, 1991). No physical parametrizations are used in the model, except a horizontal diffusion similar to the one described in Thépaut and Courtier (1991) and a simple linear scheme for representing vertical diffusion, described in the next section. In spite of these parametrizations of diffusion, we will refer to this model as the adiabatic T63 model hereafter. The numerical validation of the tangent-linear and adjoint versions of this model has been performed as described by Thépaut and Courtier (1991).

2.4 The linear parametrization of vertical diffusion.

The present experiments use a version of the model, which has linear parametrizations of diffusion and is otherwise adiabatic. Only this version of the model has an existing adjoint. The simplified vertical diffusion of Buizza (1993), which is used here, effects u and v wind components and dry static energy. (In the present experiments the diffusion does not operate on dry static energy). In general we may write the vertical diffusion equation in terms of a vertical flux divergence,

$$\rho \frac{\partial \psi}{\partial t} = -\frac{\partial F_\psi}{\partial z} \tag{4}$$

Here ψ is the u or v wind component (or dry static energy), and F_ψ is the flux of ψ. In the simplified parametrization, the fluxes are assumed to be independent of stability. Further, the density ρ and the height above the model surface z are assumed to be known fixed functions of the model vertical coordinate, derived from the ICAO standard atmosphere. In addition, a number of other variables described below are assumed to be known constants. As a consequence, the simplified vertical diffusion is strictly linear and the finite difference form of the vertical diffusion operator at a single latitude longitude grid point is simply a constant tridiagonal matrix. The specific parametrizations of the fluxes are now given.

Between any two model levels the flux is parametrized by

$$F_\psi = \rho_0 u_* L_D f(z) \frac{\partial \psi}{\partial z} \tag{5}$$

where ρ_0 is the surface density, u_* is the surface friction velocity (0.5 m/s over land; 0.2 m/s over sea), L_D is the mixing length and f is an *ad hoc* function to decrease the strength of vertical diffusion with height. We define L_D by

$$L_D = kz/(1 + kz/\lambda) \tag{6}$$

where k is von Karman's constant (0.4) and λ is the asymptotic mixing length (90 m). We take

$$f(z) = exp(-z/h_0) \tag{7}$$

where h_0 is the height of the planetary boundary layer (1 km).

At the top of the atmosphere $F_\psi = 0$. At the bottom of the atmosphere ($F_\psi = 0$ for dry static energy, but for u or v wind component) there is a surface drag of the form,

$$F_\psi = \rho_0 u_* [k/ln(z/z_0)]\psi \tag{8}$$

where z_0 is the surface roughness height (50 mm over land; 0.5 mm over sea).

2.5 The minimization procedure.

The 4dVAR minimization problem is large. At T63, with 19 levels, the number of degrees of freedom in the control variable x is more than 300000. A robust and efficient descent algorithm is required. Algorithms of this type are iterative and require an initial estimate of x. In our experiments this initial estimate is always taken to be equal to the background, x_b. To improve efficienty we precondition the problem, by defining the norm of x for the purpose of the minimization algorithm as $x^T B^{-1} x$. We use the variable-storage quasi-Newton algorithm of Gilbert and Lemaréchal (1989). The method uses available in-core memory to store recent model state and gradient increments which are then used to approximate the inverse Hessian matrix of the cost function. In the experiments presented here the initial estimate of this matrix is taken to be the identity matrix (however, due the preconditioning used, the minimization is effectively performed in a Hilbert space with metric B^{-1}), and storage is provided to allow 10 updates of the Hessian matrix. This storage is used cyclically. That is, once the memory is filled, each time a new gradient is calculated it replaces the oldest gradient still present in memory. Thus the approximate inverse Hessian matrix is always based on the most recently computed gradients.

2.6 The equivalence of 4dVAR and the Kalman filter.

It has been often stated that under certain conditions the solution of the 4dVAR problem and that of the Kalman-Bucy filter are identical (e.g. Daley, 1991). Both methods and the arguments showing this equivalence are outlined by Lorenc (1986). As noted by Daley (1991, page 384) this equivalence is exact only when

- The forecast model is linear.
- The interpolation operator H is linear.
- The forecast model is perfect.

Also the equivalence holds only for the analyses produced at t_n. That is, for any time within the analysis time period the 4dVAR solution is influenced by data throughout the time period, whereas the Kalman filter analyses at any particular time makes use only of previous data. The 4dVAR solution, under the above conditions, is better identified with the fixed interval Kalman smoother. The interested reader is refered to Jazwinski (1970, examples 7.8, 7.16), who derives the Kalman smoother from the same maximum likelihood principle which leads to the 4dVAR minimization problem.

A consequence of the theoretical equivalence between the two methods is the implicit use in 4dVAR of flow-dependent forecast error covariances. In general one expects that the application of a full Kalman filter to a 4d data assimilation problem will lead to inhomogeneous forecast error covariances since these covariances are the initial background error covariances evolved according to the linearized model dynamics. The exact transport in time of the forecast error covariance matrix is not tractable with the actual resolution of the operational models. The practical advantage of 4dVAR comes about because the forecast error covariances are not explicitly computed. However, they are implicitly used

in the 4dVAR assimilation. The single observation experiments reported here allow us to visualize the forecast error covariances of the Kalman filter equivalent to the 4dVAR.

The equivalence of 4dVAR and the Kalman filter, which provides a means of interpreting the results of our single observation experiments (Section 3), is only approximate: The forecast model is not linear, but over the 24h period the evolution of perturbations is approximately linear. (The 4dVAR solutions would be little effected if the tangent linear model were used in place of the nonlinear model). The interpolation operator is in fact very close to linear. However, here we consider only the case when the observation is of a model variable at a grid point. Finally, the forecast model is far from perfect, but we limit our comparison to a Kalman filter which ignores model errors.

First we note that for an optimal analysis x_a, such as from 3dVAR, or an idealized OI or from the analysis performed at each step of the Kalman filter, the analysis increments, $x_a - x_b$, are a linear combination of the observation increments, $y - H(x_b)$, (Lorenc, 1986, equation 28),

$$x_a - x_b = BH'^T(H'BH'^T + O)^{-1}[y - H(x_b)] \tag{9}$$

where the matrix H' is the linearization of H in the vicinity of the current state x_b. For the Kalman filter x_b is the forecast from the previous analysis and B and H are defined accordingly. In the case of a single observation, located at a model grid point, and taking the model state to be a grid point representation, H'^T becomes a vector as long as the model state vector containing all zeros except for a single one corresponding to the observation variable and location. In this special case (9) simplifies to

$$x_a - x_b = \left(\frac{y - x_{b\alpha}}{b_{\alpha\alpha} + o_{\alpha\alpha}}\right) B_\alpha \tag{10}$$

where α indexes the observation in the model state vector so that $b_{\alpha\alpha}$ is the background covariance of the observation variable and location, $o_{\alpha\alpha}$ is the observation variance and B_α is the column of B corresponding to the observation variable and location. This shows that the analysis increments are proportional to B_α, i.e. to the covariance of the background error at observation variable and location with the background error of all other model variables and locations. Note that (10) shows that at the observation location, the analysis increment is smaller in magnitude than the observation increment. However depending on the structure of B_α the analysis increments at other locations can be larger than the observation increment.

This relationship also holds for the 4dVAR solutions at t_n in our single observation experiments because the 4dVAR solution at t_n is equivalent to the corresponding Kalman filter solution for this problem. The corresponding Kalman filter is one in which there are no model errors and no other observations. In such a case the only actions of the Kalman filter until the final analysis are to advance the model state and the error covariances of the model state to t_n. Thus the 4dVAR solution for a single observation at t_n is a column of the predicted covariance matrix of the corresponding Kalman filter. This covariance matrix is predicted using linear dynamics, which simplifies in this case to

$$B(t_n) = RB(t_0)R^T \tag{11}$$

where R is the tangent linear model dynamics for the period $[t_0, t_n]$.

To date no one has applied the Kalman filter to an atmospheric model (nor to any other model) with 300000 degrees of freedom. However, thanks to the analysis presented here, the results of Section 3 demonstrate just how complex the predicted error covariances can become in such a case, in just 24 h. This very complexity has important implications for the eventual implementation of the Kalman filter—any approximations made in modeling the covariances must still be capable of representing very complex structures.

2.7 Finite time optimal modes.

In Section 3 we will compare the evolution of the 4dVAR increment patterns during the analysis period with rapidly growing perturbations of the atmospheric dynamics for the specific meteorological situation. To measure the perturbation we use the energy norm as defined by Rabier and Courtier (1992, equation 11). Since our problem is limited in time and the tangent linear model evolution is not represented by a symmetric matrix, exponentially growing normal modes do not maximize the growth of the perturbation. Instead we study so-called optimal modes (Lacarra and Talagrand, 1986; Farrel, 1989), which maximize linear disturbance growth over a given time period (Molteni and Palmer, 1991). As shown by these authors, these optimal modes are the eigenvectors associated with the largest eigenvalues of the operator R^*R, where R is the tangent linear model of (11), and R^* is the adjoint of R, for the norm used to measure the perturbation growth.

Within the IFS system, a Lanczos algorithm (Simon, 1984) has been developed to compute these optimal modes (Buizza, 1992). For computational cost reasons, the modes are computed at a T21 resolution, but horizontal diffusion is suppressed in the model to avoid excessive damping of the small scales. The vertical diffusion of Section 2.4 is retained in these calculations.

3 Single observation experiments.

As discussed in Section 2.6, 4dVAR implicitly evolves the background covariances in time. Thus in contrast to simplified sequential assimilation schemes such as 3dVAR, 4dVAR is able to implicitly specify flow-dependent covariance functions. Here we study the case of the small intense storm which caused extensive damage in Brittany and southwestern England on 16 October 1987 (Jarraud et al., 1989). We find that within 4dVAR, a single key datum, indicating the position and intensity of a developing storm, can have a very significant impact.

Section 2.6 also shows that the analysis increments from a single datum are proportional to the error covariance of the background. For 3dVAR, this error covariance is designed to be nearly identical to the forecast error covariances used in the conventional OI (Heckley et al., 1992). The OI covariances are themselves fairly homogeneous and isotropic in the horizontal, with simple correlations in the vertical and between variables (Shaw et al., 1987; Undén, 1989; and references therein). In our 4dVAR experiments the background covariances used at t_0 are identical to the constant in time 3dVAR background covariances. In 4dVAR, these covariances evolve implicitly, as described in Section 2.6, becoming extremely complex by t_n.

In these experiments, the analysis increments appear to be closely connected to the optimal modes of Section 2.7. An informal argument why this must occur follows: Any initial state perturbation can be thought of as projecting on the initial states of the optimal modes, i.e., the eigenvectors of Section 2.7. The 4dVAR solution will naturally tend to project primarily on the fastest growing modes. Consider for example, a mode which decays in time. The 4dVAR solution perturbation might have a projection on such a mode, but that part of the 4dVAR solution will decay with time and have negligible effect on the observations part of the cost function. It will however inflate the background part of the cost function. Therefore the initial state projection on the decaying modes should be zero. Conversely, rapidly growing modes can have large effects on the observations part of the cost function, with quite small effects on the background part of the cost function.

3.1 A height observation at 250 hPa.

In this experiment and in the experiment of Section 3.2, the background field is a 6 hour forecast, taken from a T63 OI assimilation cycle, valid at 00 UTC 15 October 1987. Fig. 1 presents the 24 hour evolution of the background 500 hPa height and mean sea level pressure fields. The adiabatic T63 model forecast shown here is poor, considering that the intensity and the location of the actual storm was a minimum low pressure of 951 hPa between Brittany and Cornwall at 00 UTC 16 October 1987. However, for our purpose, the rapid evolution of the dynamics of the model during the assimilation period is more important than the forecast skill. In particular note the strong deepening of the 500 hPa trough, and the movement and deepening of the surface low from 985 hPa at 20°W–43°N to 978 hPa at the tip of Brittany (5°W–49°N). During this period, the vertical tilt of the low between the surface and 500 hPa is typical of a rapidly intensifying baroclinic situation.

In the assimilation experiment we include only a single geopotential height observation located in the trough at 250 hPa (5°W–44°N) at the end of the period. The observation increment (observation minus background) is −70 meters, with an expected standard deviation of 12 meters. The minimization procedure is allowed to continue until the norm of the gradient of J is reduced by a factor of 1000.

Fig. 2 shows the geopotential height and wind analysis increments (analysis minus background) at the end of the assimilation period for 250, 500, 850, and 1000 hPa. Clearly the analysis increments are not isotropic. While the maximum amplitude of −76 m is obtained at 250 hPa in the vicinity of the observation, there is an important west-east propagation of the information consistent with the dynamics of the model for this situation, leading to a second extremum of opposite sign (+39 m) near 20°W–40°N. Both extrema propagate vertically down to 850 hPa, the vertical tilt of the positive extremum between 850 and 500 hPa is consistent with lower troposphere baroclinic instability of this meteorological situation.

As a comparison to the 4dVAR results we perform a simple equivalent 3dVAR data assimilation. Having only one observation at the end of the assimilation period, the analysis differs from the background only at this time. The resulting increments (Fig. 3) correspond exactly to the spatial structure of B. When compared with Fig. 2 and the

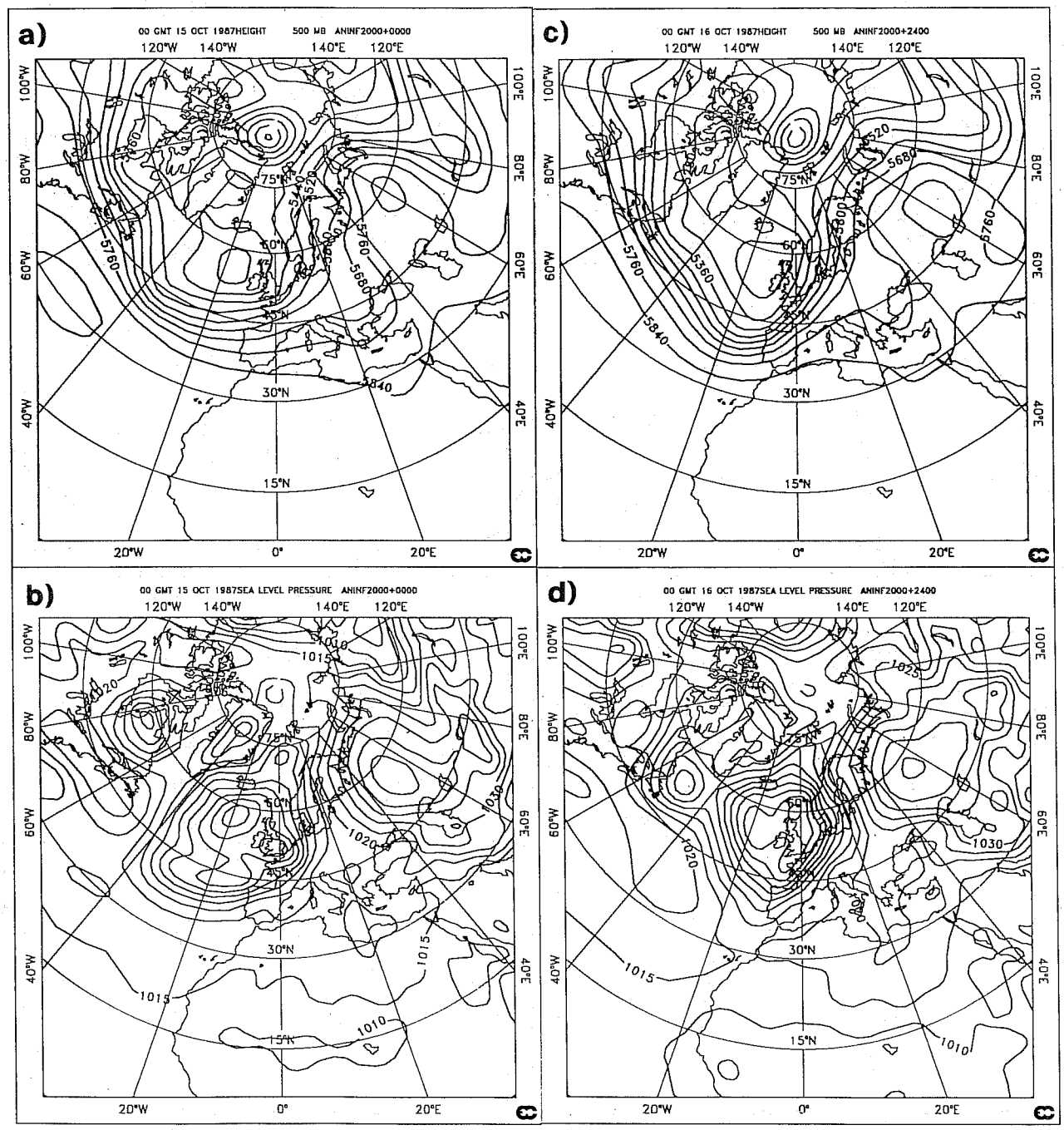

Fig. 1 Background fields for 00 UTC 15-16 October 1987. Shown here are the Northern Hemisphere (a) 500 hPa geopotential height and (b) mean sea level pressure for 15 October and the (c) 500 hPa geopotential height and (d) mean sea level pressure for 16 October. The fields for 15 October are from the initial estimate of the initial conditions for the 4D-Var minimization. The fields for 16 October are from the 24 hour T63 adiabatic model forecast from the initial conditions. Contour intervals: 80 m and 5 hPa.

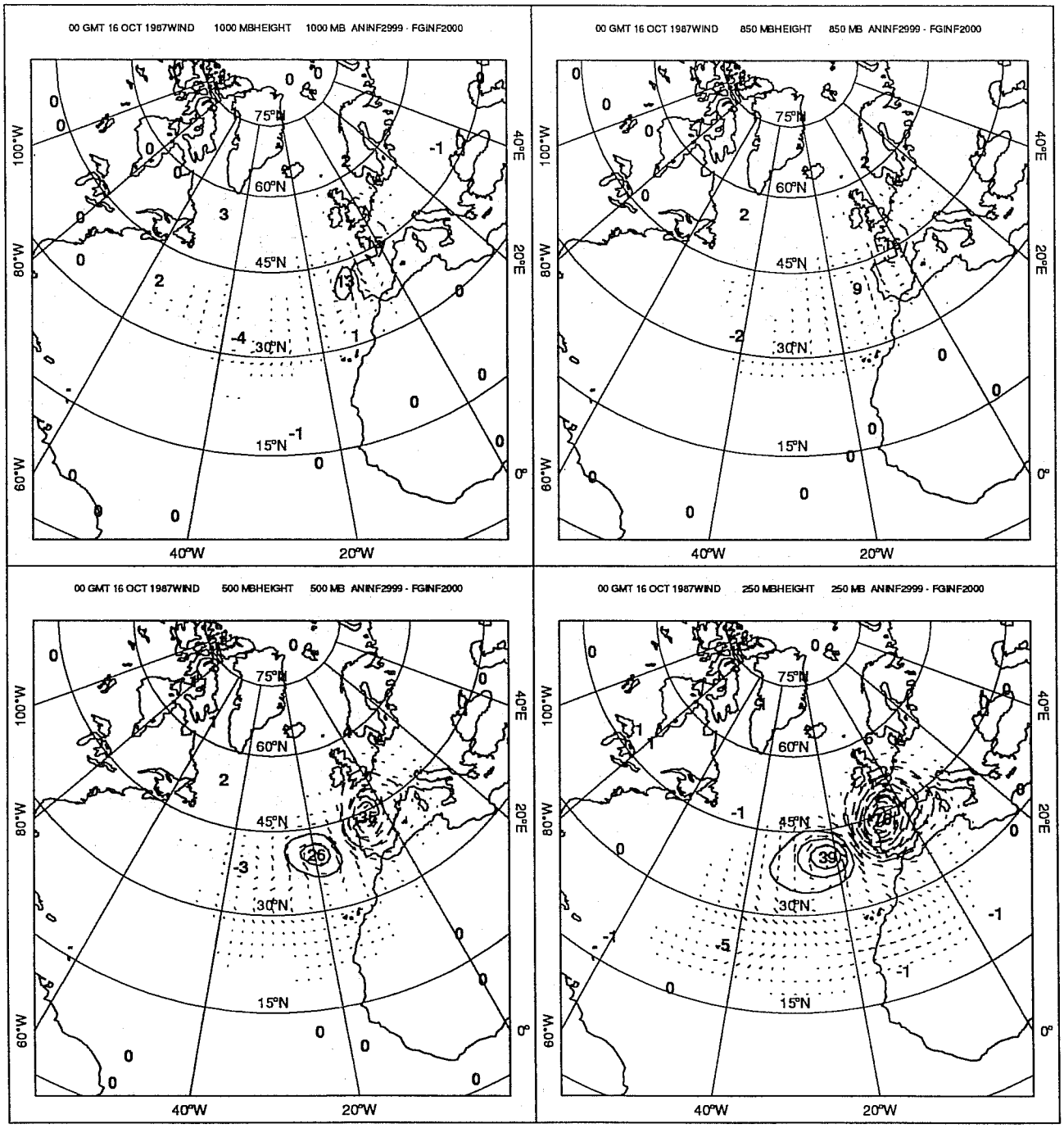

Fig. 2 The 4D-Var analysis increments (analysis - background), at the end of the 24 hour assimilation period, for geopotential height and wind at 250, 500, 850 and 1000 hPa, corresponding to a single height observation at 250 hPa. Contour interval: 10 m.

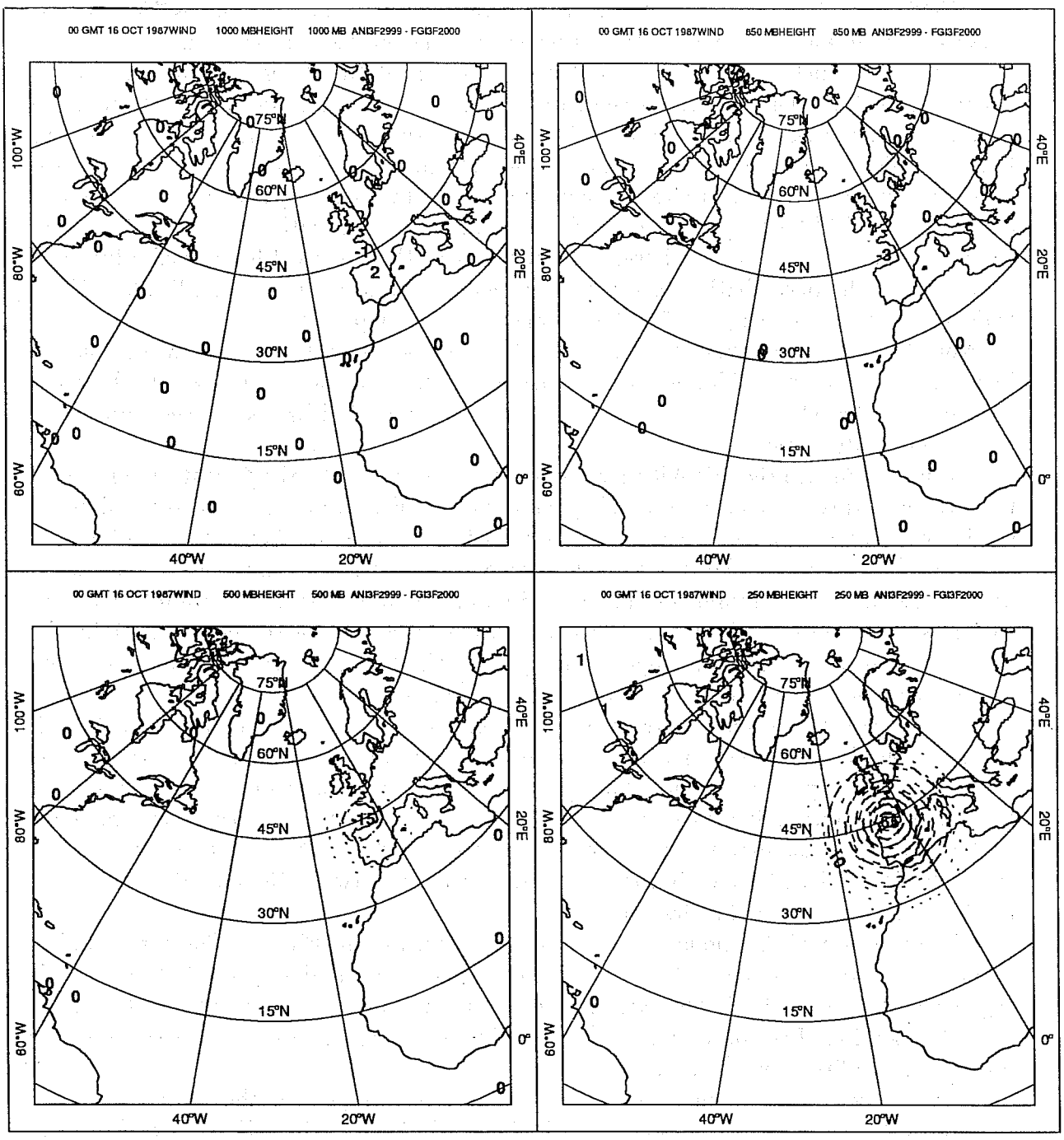

Fig. 3 As in Fig. 2 but the 3D-Var analysis increments at the end of the assimilation period. Contour interval: 10 m.

evolution of the dynamics presented in Fig. 1, one can see that isotropic and barotropic covariance functions are poorly adapted for such a meteorological situation.

The 4dVAR method, being a smoother, spreads the data influence both forward and backward in time. The 4dVAR increments 24 hours before the observation are shown in Fig. 4. These increments at the initial time are quite small, within the uncertainty of our best analysis, and similar in magnitude to the data misfit at the final time. One can see that the increments propagate horizontally with basic state steering current. The negative extremum at 500 hPa at t_n is 20° east of that at t_0, consistent with Fig. 1. In addition to the baroclinic signature in the lower troposphere and the eastward horizontal advection, we note that the perturbation propagates vertically with a maximum amplitude shifting from 400 hPa (not shown) to 250 hPa during the 24 hour period.

Note that the single height observation leads to balanced height and wind analysis increments at all times. The mass-wind balance at t_0 is a result of using a background covariance B based on a balance relationship. This mass-wind balance is then preserved by the model dynamics.

We now compare the 4dVAR increments (Figs. 2 and 4) to the fastest growing perturbations of this particular meteorological situation. Fig. 5 presents the vertical cross-section of the norm of the first 6 eigenvectors of the operator R^*R at time t_0 and after a 24 hour linear evolution. For the first three eigenvectors, the maximum energy is located near model level 11 (around 500 hPa) at time t_0 and model level 8 (around 250 hPa) 24 hours later. The amplification factor (i.e. the square root of the eigenvalue) for the three most unstable modes is approximately 4 for the 24 hour period. Thus any linear combination of the first three eigenvectors is unstable with this growth rate.

Fig. 6 presents the spatial structure of the first eigenvector at time t_0 for 1000, 850, 500 and 250 hPa for the stream function field. This most unstable mode as well as the two subsequent eigenvectors (not shown), are localized in our area of interest. As seen in Fig. 5, the amplitude is maximum at around 500 hPa. At this level there is a negative pattern over Newfoundland, a positive one located at 40°W–50°N and another negative one at 20°W–50°N. The shift in location of the extrema between 500 and 850 hPa shows the baroclinic nature of this first mode.

The structure of the mode 24 hours later is presented in Fig. 7. The maximum of amplitude is now at about 250 hPa. The negative pattern previously located at 20°W is larger and located at 4°W. The two other extrema have also moved rapidly eastward. In fact, the location of the observation for the assimilation experiment is the position of the maximum amplitude of this mode at this time.

There is certainly a visual agreement between the shape and the evolution of the most unstable mode (Figs. 6 and 7) and of the 4dVAR solution (Figs. 4 and 2) over this assimilation period. One cannot expect a perfect match since the first eigenvector spans only part of the unstable subspace described by the first three unstable modes. In particular, the location of the extrema for the next two eigenvectors are shifted 5° westward. However, some features match up well. In particular, at t_n the secondary positive extremum of the 4dVAR solution corresponds quite well to the positive pattern of the mode at (20°W–40°N), except that for the mode, the positive perturbation extends further west. At t_0, the spatial structure of the increments, inferred by the observation

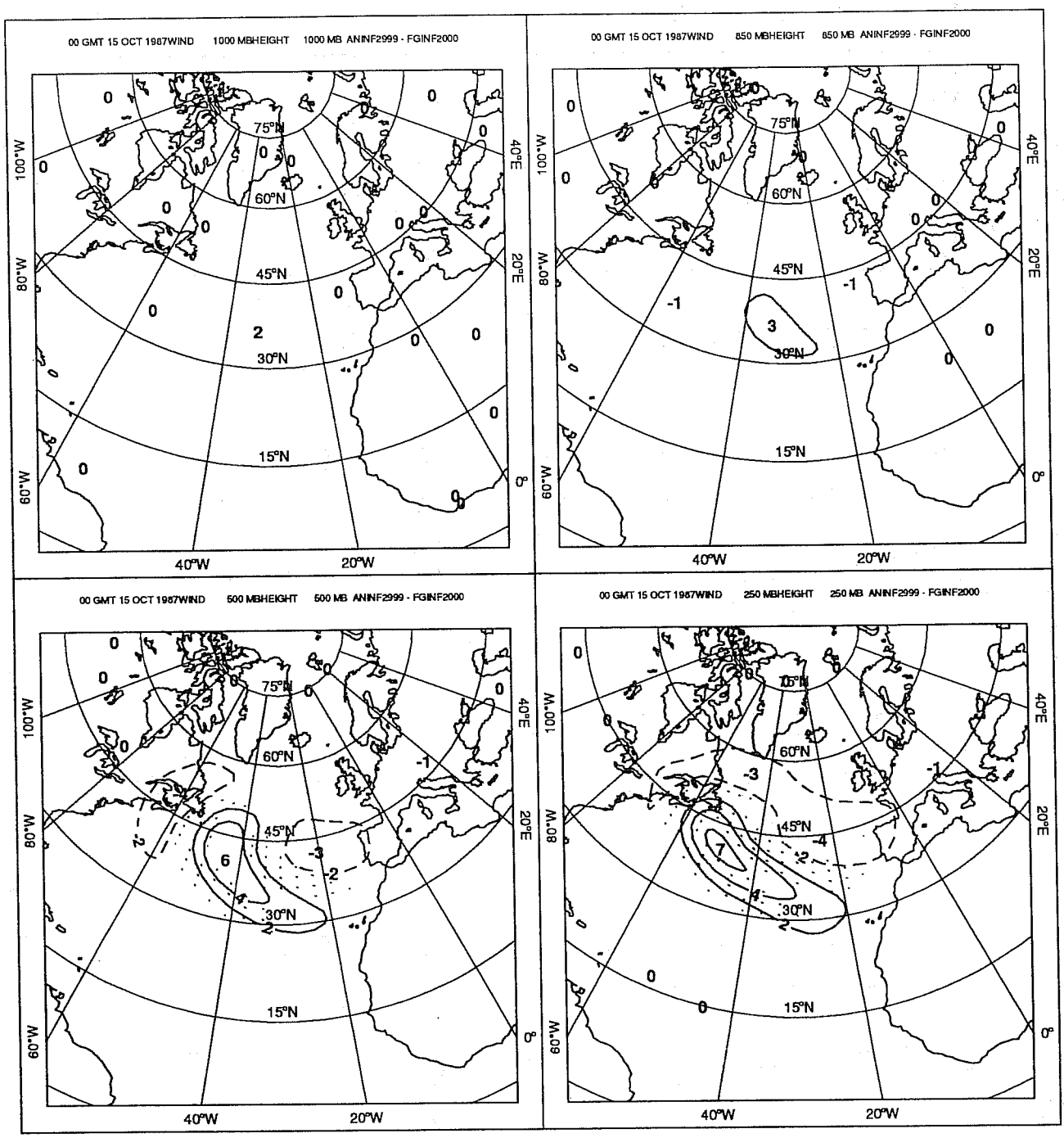

Fig. 4 As in Fig. 2 but the 4D-Var analysis increments at the beginning of the assimilation period. Contour interval: 2 m.

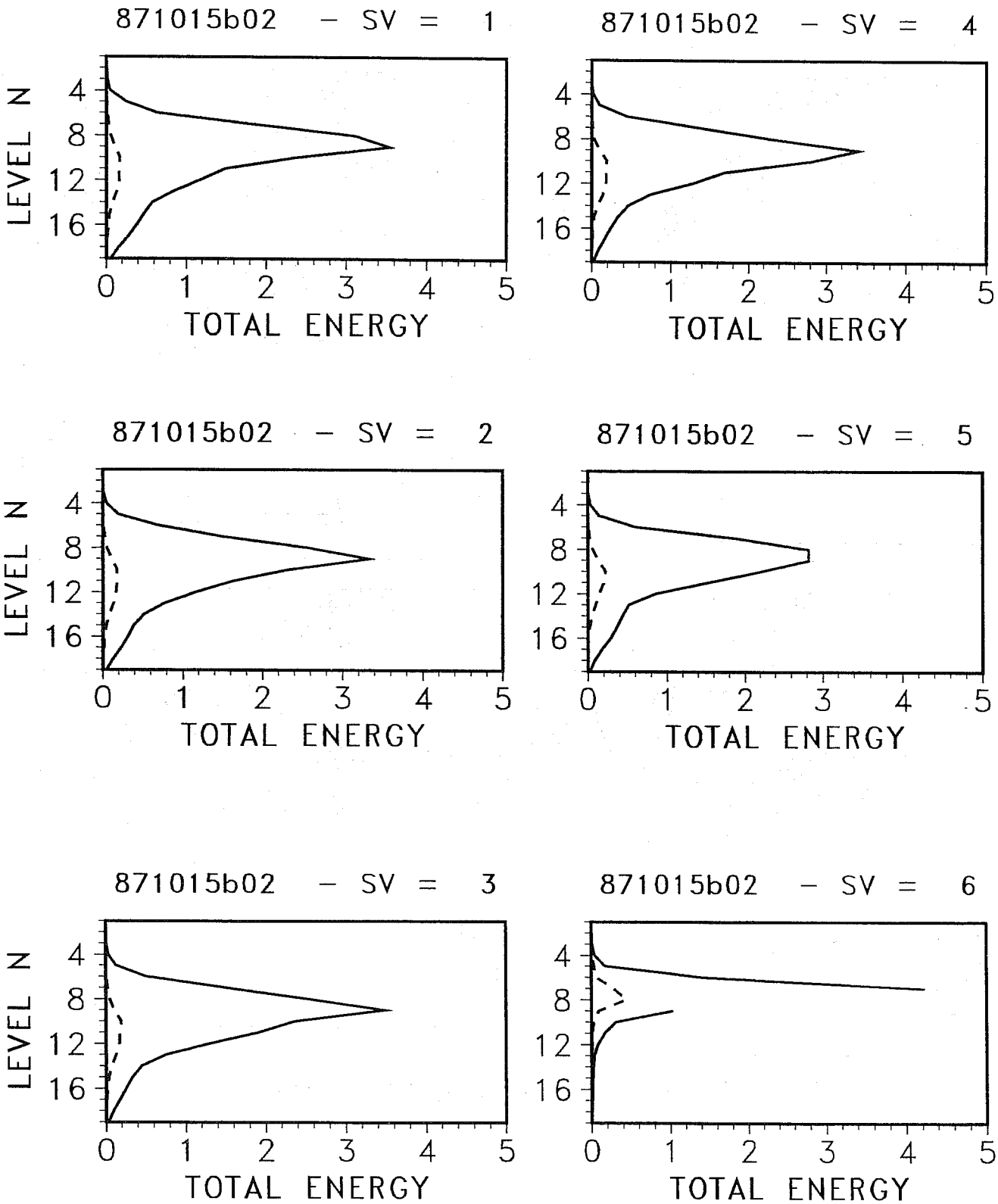

Fig. 5 Vertical cross-section of the energy norm of the first six eigenvectors of the operator $R^{*}R$ at the initial time (dashed line) and after a 24 hour tangent linear integration (solid line).

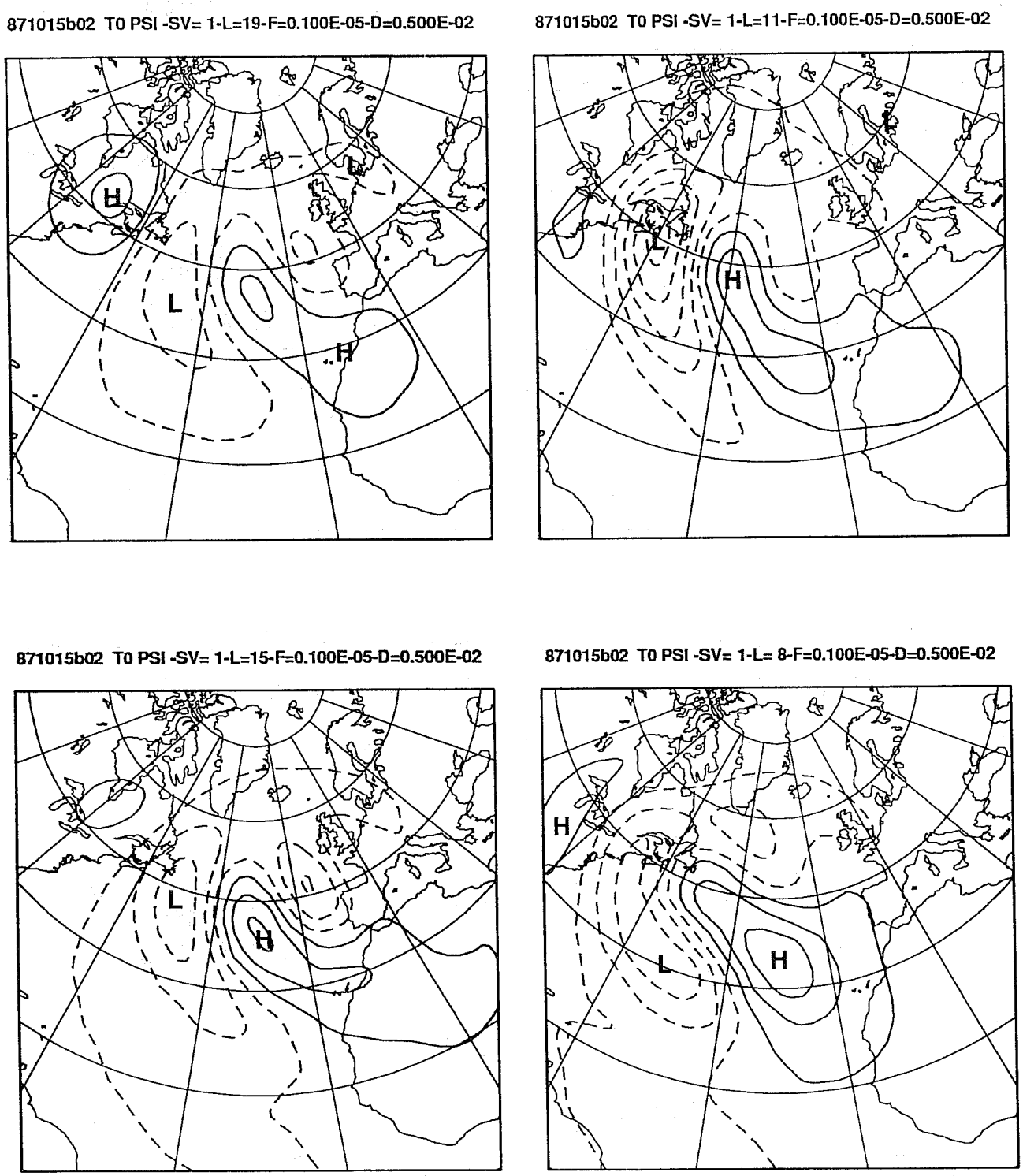

Fig. 6 Streamfunction at roughly 250, 500, 850 and 1000 hPa (respectively model levels 8, 11, 15 and 19) of the most unstable mode at the initial time. Contour interval: $.510^4 m^2.s^{-1}$.

871015b02 TEND PSI -SV= 1-L=19-F=0.100E-05-D=0.200E-01

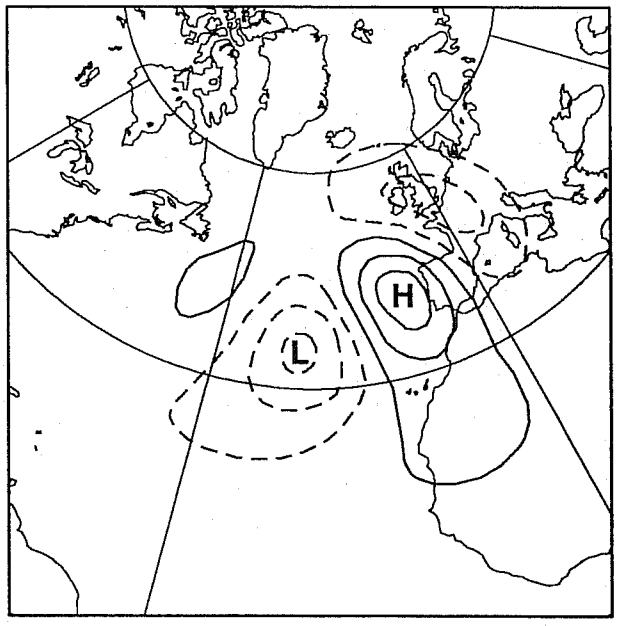

871015b02 TEND PSI -SV= 1-L=11-F=0.100E-05-D=0.200E-01

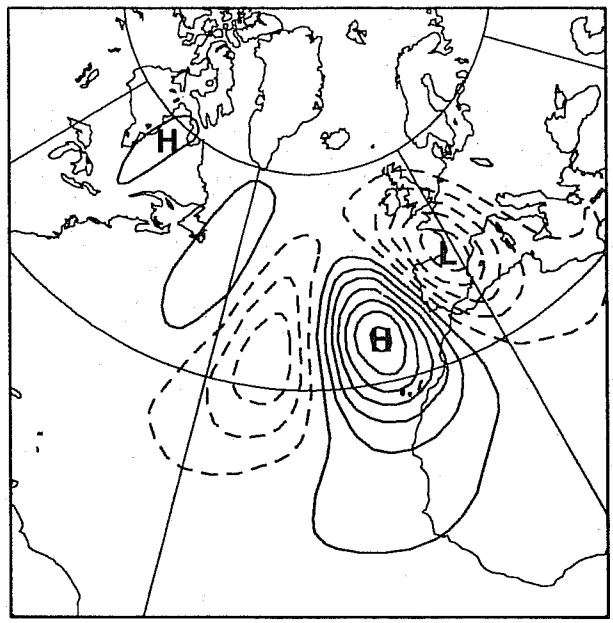

871015b02 TEND PSI -SV= 1-L=15-F=0.100E-05-D=0.200E-01

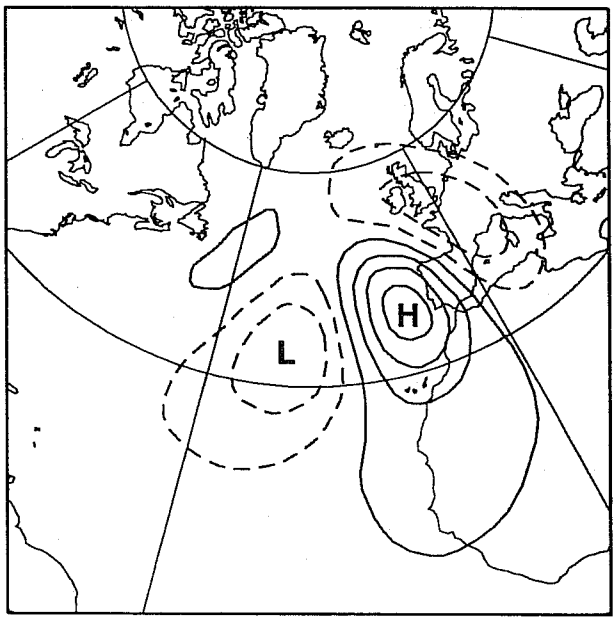

871015b02 TEND PSI -SV= 1-L= 8-F=0.100E-05-D=0.200E-01

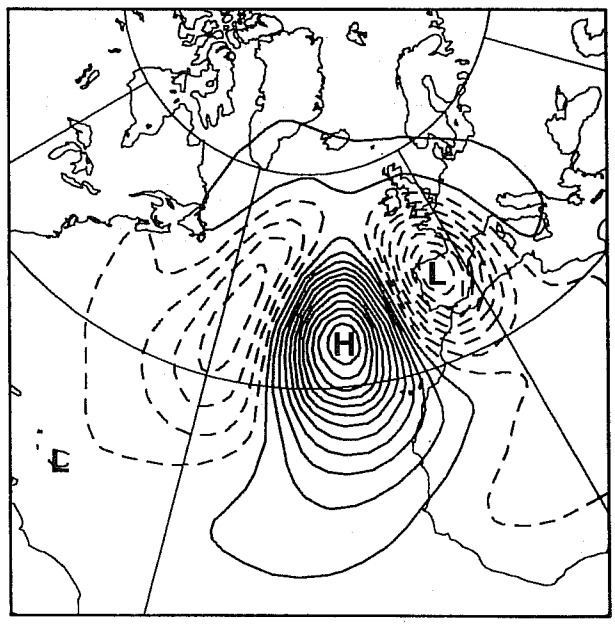

Fig. 7 As in Fig. 6 but after a 24 hour tangent linear integration. Contour interval: $.210^{4}m^{2}.s^{-1}$.

present 24 hours later, corresponds roughly to the shape of the unstable mode. The location of the extrema is, in particular, quite similar.

3.2 A wind observation at 1000 hPa.

This experiment parallels that of Section 3.1, except that here a single zonal wind observation is inserted at 1000 hPa. The observation location is again 5°W–44°N. The u-wind increment is 20 m/s. The observational standard deviation is 3 m/s. The resulting analyses are presented in Figs. 8, 9 and 10, which are analogous to Figs. 2, 3 and 4 presented in Section 3.1.

First considering Fig. 8, the impact is largest at 250 hPa, the level of the maximum amplitude of the optimal mode, not at 1000 hPa, the level of the observation. Also the pattern of the 4dVAR analysis increments at 250 hPa are very similar to the previous case, but shifted a few hundred km eastward. As in Fig. 2, the dipole pattern at 250 hPa persists in the vertical, but now rotates counterclockwise with increasing pressure, completing the near quarter turn necessary to match the wind observation. The decay of amplitude with increasing pressure is less in this case. The 3dVAR results (Fig. 9) again faithfully represents the simple background covariances. The largest 3dVAR impacts are restricted to the levels near the data level.

At the initial time, the 4dVAR analysis increments (Fig. 10) are quite different than in the case of the height observation. Since that data location does not match the location of the maximum amplitude of the optimal modes, a larger initial amplitude is required. The vertical structure of the initial perturbation is much more complex, with a positive extrema at 500 hPa and a negative extrema at 850 hPa. The patterns at these two levels are similar in shape and amplitude but of opposing sign. At other levels, particularly at 1000 hPa, increments are small.

4 Impact of ERS1 scatterometer σ^0 observations.

The result that the impact of a surface wind observation can increase with height (Section 3.2) suggests that the impact of scatterometer observations may be substantial in 4dVAR. Two 4dVAR assimilation experiments are described here for the 24 hour period 12 UTC 30–31 December 1991. As mentioned in the Introduction a violent storm struck the coast of Norway 24 hours later. The first experiment, referred to as CONTROL, uses all conventional upper air observations. Vasiljevic et al. (1992) describe the handling of these observations within the IFS system. A second experiment, referred to as SCATT, is identical to CONTROL except that scatterometer σ^0 observations are added as described in Section 2.2.

This case is chosen for study because of the intrinsic interest of the 1992 New Year's Day storm and because a preliminary study of the impact of scatterometer winds in the operational OI assimilation had previously been performed at ECMWF for the period from 00 UTC 26 December 1991 through 2 January 1992 (Hoffman, 1993). The conclusions of that study are:

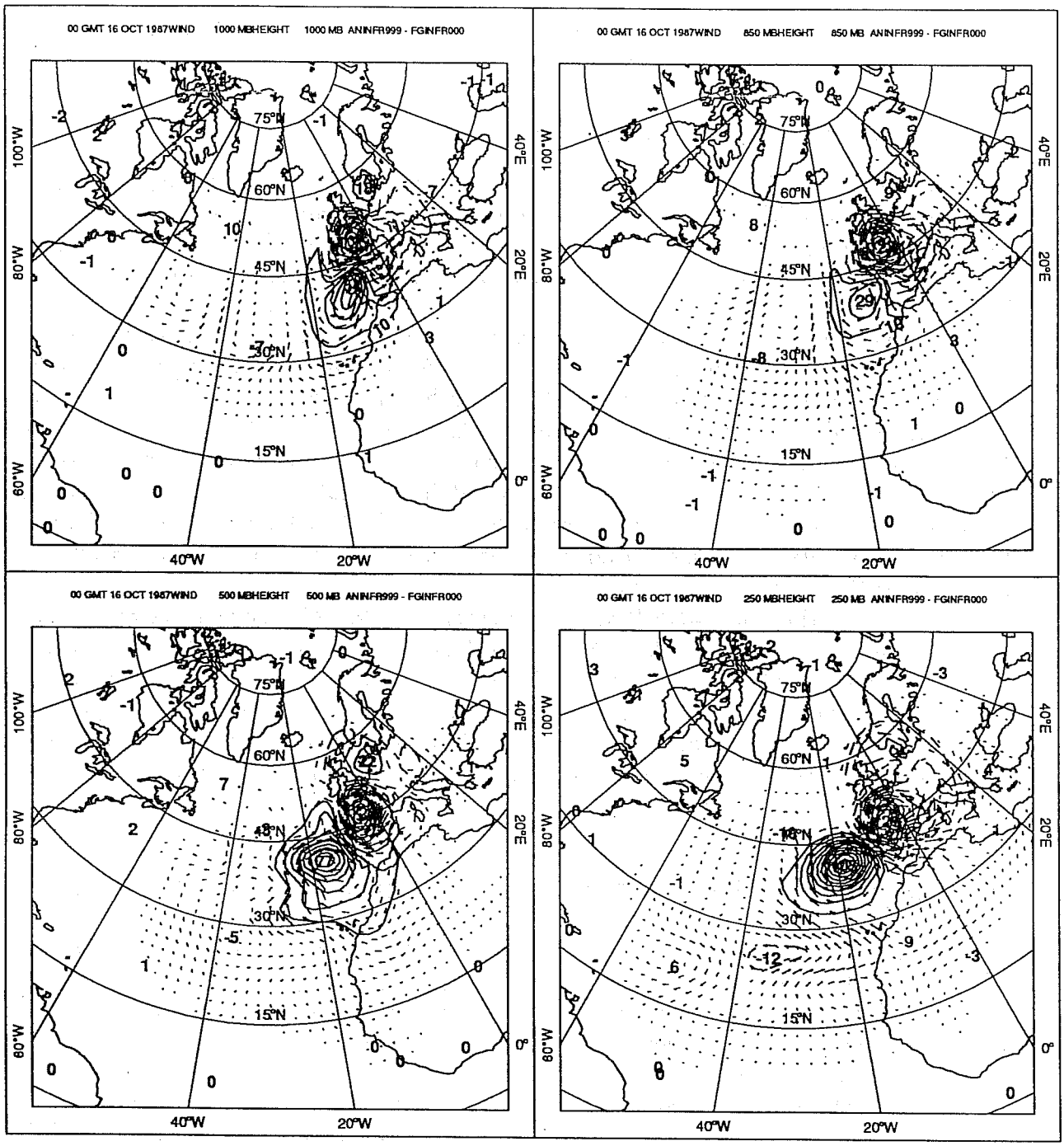

Fig. 8 . The 4D-Var analysis increments (analysis - background), at the end of the 24 hour assimilation period, for geopotential height and wind at 250, 500, 850 and 1000 hPa, corresponding to a single wind observation at 1000 hPa. Contour interval: 10 m.

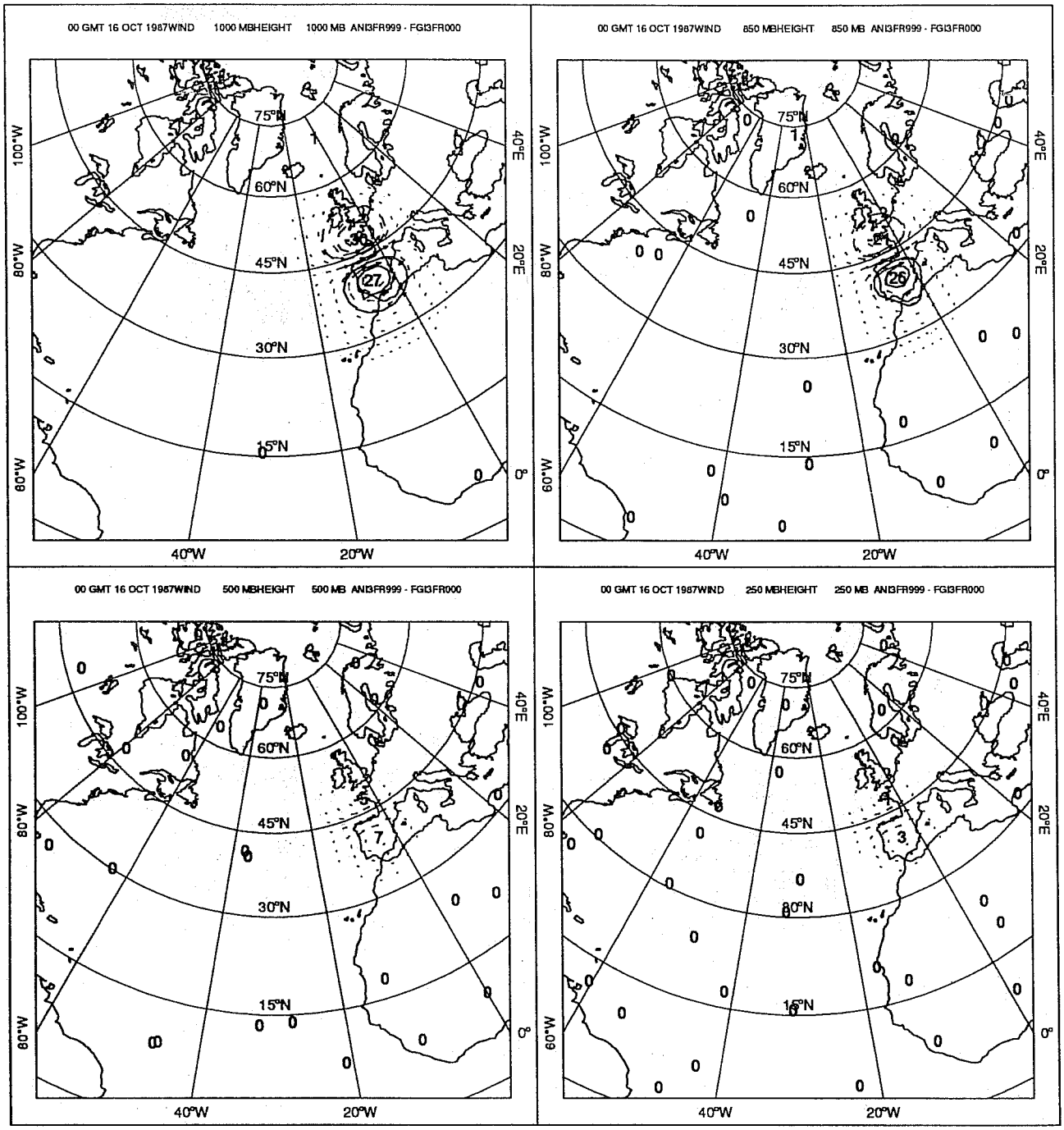

Fig. 9 As in Fig. 8 but the 3D-Var analysis increments at the end of the assimilation period. Contour interval: 10 m.

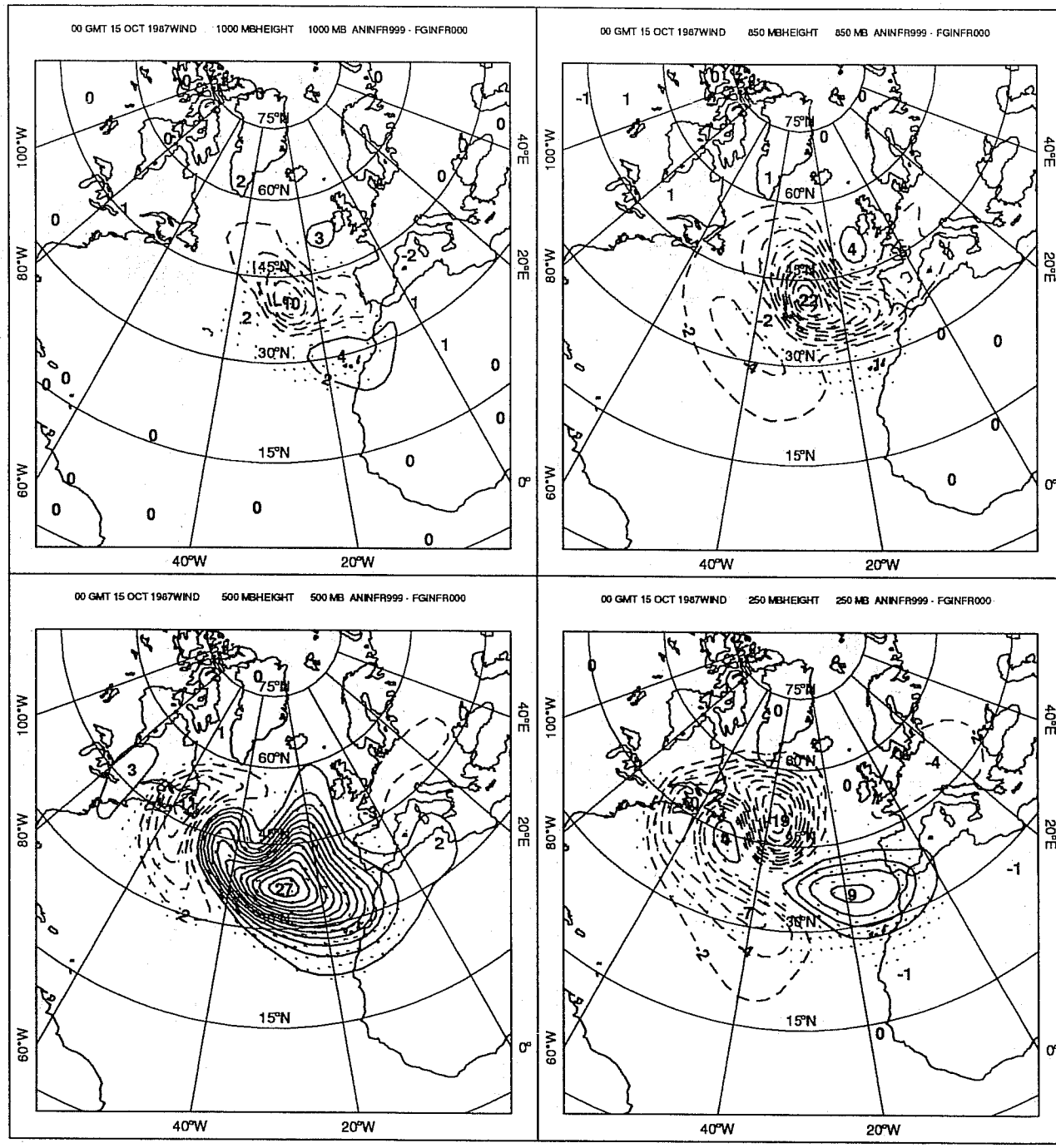

Fig. 10 As in Fig. 8 but the 4D-Var analysis increments at the beginning of the assimilation period. Contour interval: 2 m.

- The impact of the data on the assimilation is weak.
- The analysis draws to the data without producing associated changes to the mass field.
- The analysis changes decay in the subsequent 6 hour forecast.
- The ambiguous nature of the scatterometer winds requires strong quality control.

The present experiment tests the performance of 4dVAR for the same situation, although with a simplified forecast model. The advantage of the variational approach is that it embeds the ambiguity problem in a large data fitting problem which includes other observations, a background constraint based on balanced error covariances and the model dynamics. The last two factors lead necessarily to a dynamically consistent use of the data.

In both CONTROL and SCATT we add a weak constraint on the gravity waves as in Courtier and Talagrand (1990). Also in both cases the minimization is stopped after 30 iterations. In SCATT, the σ^0 are quality controlled in the sense that they are rejected if the sea surface temperature at the observation location is less than 274.5 K or if the analyzed 10 m wind speed (from the SCATT experiment of Hoffman (1993)) is less than 4 m/s.

In spite of the complexity of J_{scat}, no convergence problems are encountered during the minimization. In the SCATT assimilation, the distance between the model solution and the σ^0 data decreased substantially after 30 iterations (by a factor of 2.2 for the normalized standard error) while the fit of the other observations is hardly changed relative to that of CONTROL. During the minimization process, the part of the cost function due to the observations decreases rapidly at first and then more slowly. The full cost function has the same quasi-exponential decaying behavior because the observations dominate the cost function. The part of the cost function due to the background is initially zero and grows during the course of the minimization, but is always an order of magnitude smaller than the part due to the observations. The part of the cost function due to the constraints remains fairly constant during the minimization but is smaller still, roughly two orders of magnitude smaller than that due to the data.

The data used in the present experiment in addition to the ERS1 $sigma^0$ observations are radiosonde, pilot balloon, aircraft, and satellite cloud track wind observations; drifting buoy surface pressure observations; and radiosonde temperature and humidity observations. Conventional surface observations and satellite temperature and humidity profiles are not used. The treatement of the observations, other than scatterometer observations, in our experiments is the same as in Thépaut et al. (1993). In our experiments the scatterometer data are the most numerous data at the surface, since the number of drifting buoys is small and the conventional surface observations are not used. Also at times other than the four synoptic times, the scatterometer data are often the most numerous data type, even exceeding the total of all other data occasionally during the assimilation. In the Southern Hemisphere and Tropics the scatterometer data and cloud drift winds dominate the other data types. In the vertical the number of radiosonde and pilot balloon observations is a maximum at 850 mb, decaying slowly through the troposphere and

lower stratosphere, while aircraft reports concentrate around 250 hPa, and the majority of satellite winds occur at 850 hPa. Typical temporal and geographic data coverage is presented by Thépaut et al. (1993) (Table 1 and Figure 1).

Fig. 11 presents the mean sea level pressure field for the 4dVAR SCATT and CONTROL assimilations and the difference of the two at the end of the assimilation period. As expected, the impact is large in the Southern Hemisphere, with differences of up to 10 hPa southwest of Africa. Substantial differences can also be observed in the Northern Hemisphere, especially in the North Atlantic. Generally the σ^0 data strengthen the activity of the effected systems. This can be seen, for example, southwest of Africa, southwest of South America, and southwest and northeast of Iceland. At 500 hPa (not shown) the impact is still quite large. Again, the systems are intensified in the SCATT assimilation.

The area near Iceland is of particular interest since at 12 UTC 31 December 1991, the New Year's Day storm was forming southwest of Iceland. Subsequently, this storm grew and rapidly evolved, striking the Norway coast 24 hours later. Also there is fairly good σ^0 data coverage over this area at the end of the assimilation period. We have compared the performances of SCATT and CONTROL analyses with several manual operational analyses made by the Icelandic, Norwegian and British Meteorological services. Fig. 12 presents the analyzed mean sea level pressure, valid at this time, over the North Atlantic produced by SCATT, CONTROL, the operational ECMWF T213 analysis and the manual analysis of the UK Meteorological Office. West southwest of Iceland, SCATT strengthens the low with a substantial increase of the pressure gradient at (25°W–50°N). This seems consistent with the operational analysis. More questionable is the presence of the ridge between Greenland and Scandinavia and the two lows north of Iceland in both 4dVAR runs and especially in SCATT which creates two isolines at 972 hPa. This low pressure area is less marked in the operational analysis. The solution adopted by the UKMO analysts is somewhere in between.

Evidence in support of the 4dVAR analyses comes from the TOVS AVHRR imagery. Fig. 13 indicates a vortex northeast of Iceland at 12 UTC which intensifies in the next 6 hours. This feature is better represented in the 4dVAR assimilations than in the operational analysis. Furthermore, the σ^0 data have a beneficial impact, strengthening the analyzed low.

We now consider several 12 hour forecasts valid 00 UTC 1 January 1992. Fig. 14 displays the forecast mean sea level pressure field from the SCATT and CONTROL 12 hour adiabatic T63 forecasts and from the T213 operational suite. The verifying operational T213 analysis is also shown. We cannot expect a particularly accurate forecast with a adiabatic T63 model; rather we are interested here in the robustness of the impact of the σ^0 data in the short-range forecast.

Considering first the low northeast of Iceland, which corresponds to the vortex on the imagery. This feature rapidly grows and moves eastward. An isolated low of 960 hPa is forecast by the 4dVAR analyses, with sharper gradients in the SCATT case, while the operational forecast leads to a broad isoline of 968 hPa. The operational analysis produces an isolated low of 964 hPa. The SCATT forecast, seems to deepen the low slightly too much. This is perhaps due to the fact that the CMOD2 model function used here tends to overestimate strong winds (Stoffelen, pers. com.).

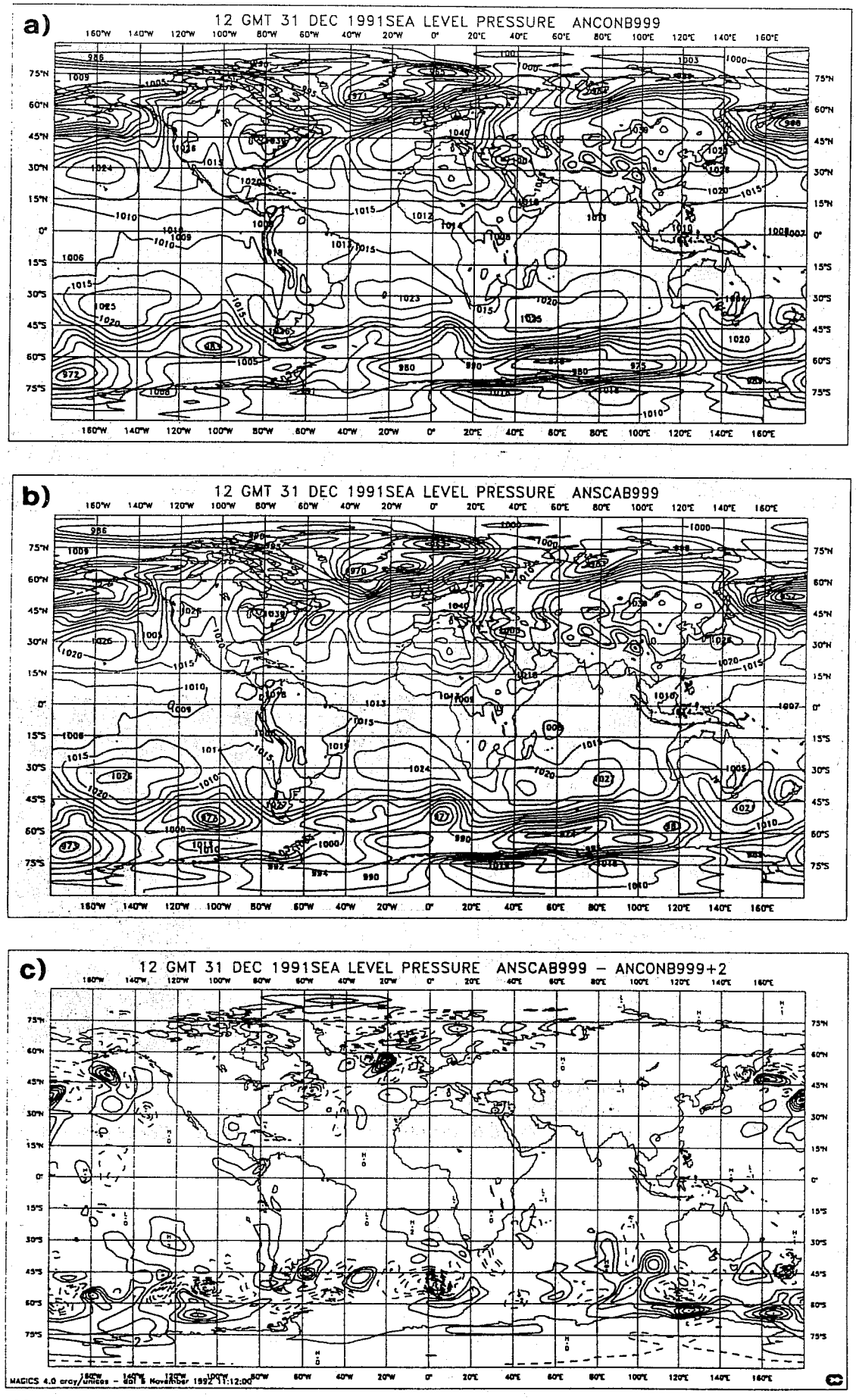

Fig. 11 Mean sea level pressure at the end of the assimilation period (12 UTC 31 December 1991) for (a) the SCATT assimilation, (b) the CONTROL assimilation and (c) for SCATT - CONTROL. Contour intervals: 5 hPa for the fields and 1 hPa for the differences.

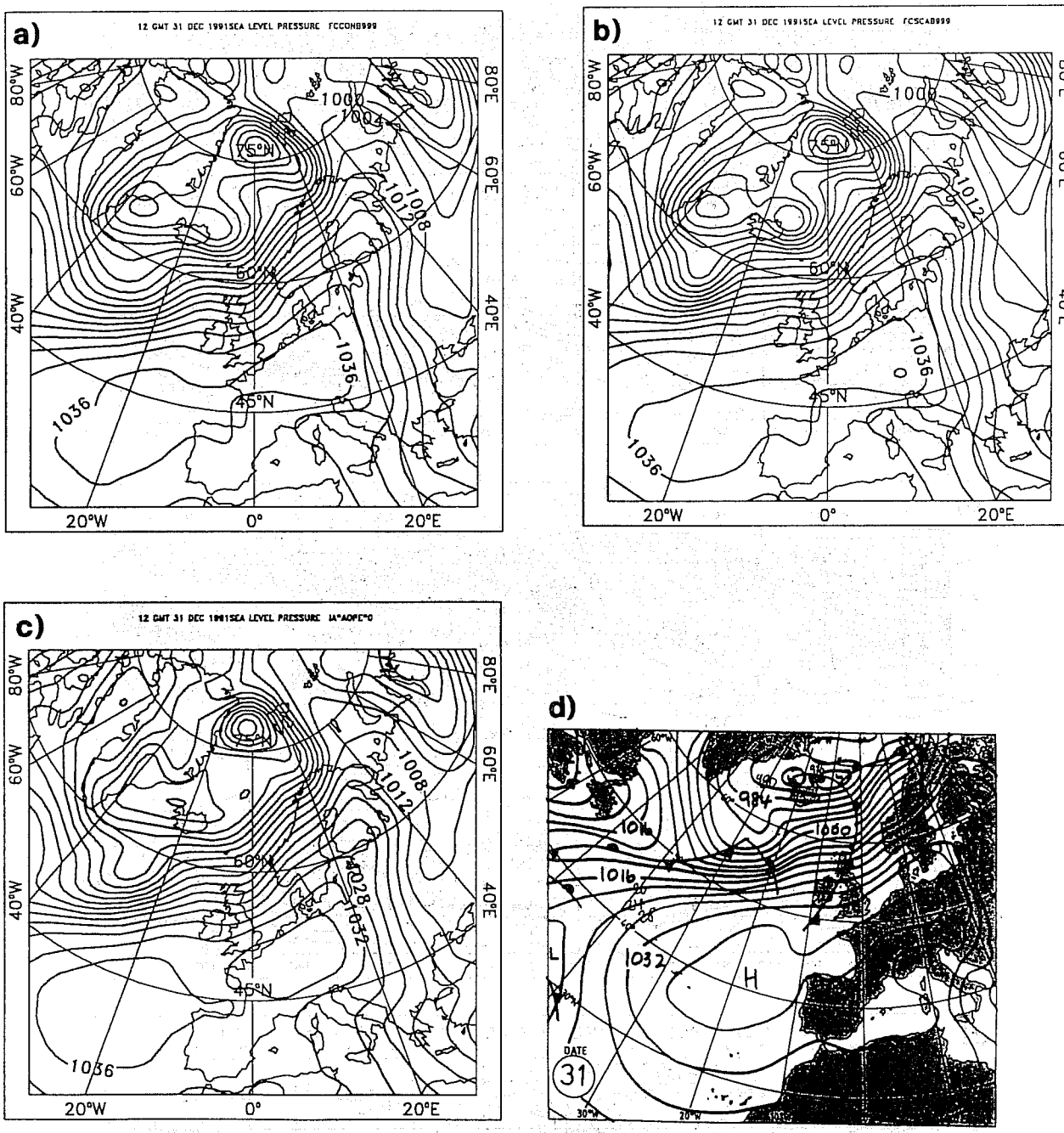

Fig. 12 Mean sea level pressure analyses valid 12 UTC 31 December 1991) from (a) the SCATT assimilation, (b) the CONTROL assimilation, (c) the ECMWF T213 operational suite and (d) the UKMO (subjective) analysis (from Weather, 1992, Vol. 47, No. 2, published by the Royal Meteorological Society). Contour interval: 4 hPa.

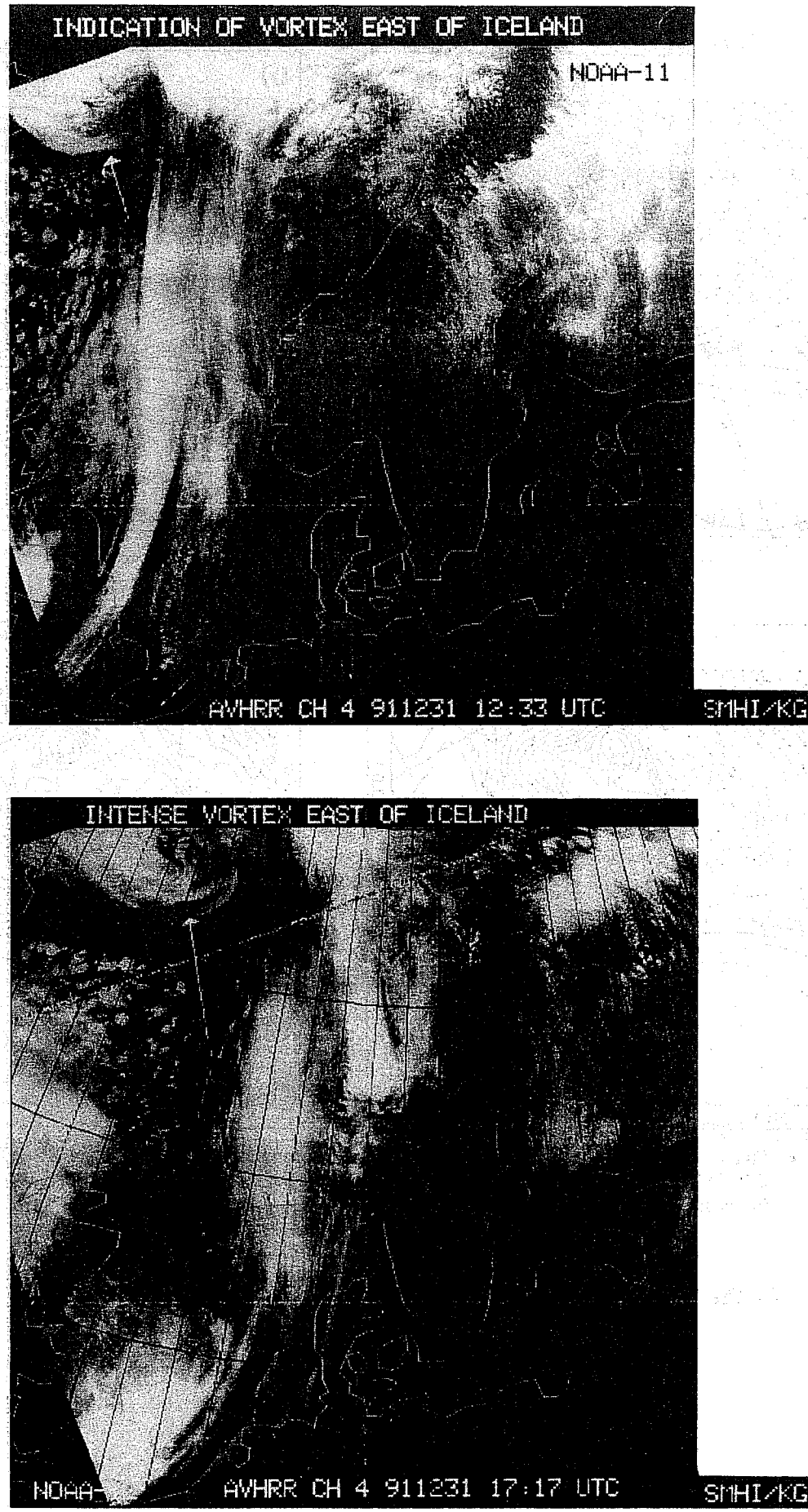

Fig. 13 Infrared imagery from AVHRR channel 4 at 1233 UTC (top) and 1717 UTC (bottom) 31 December 1991.

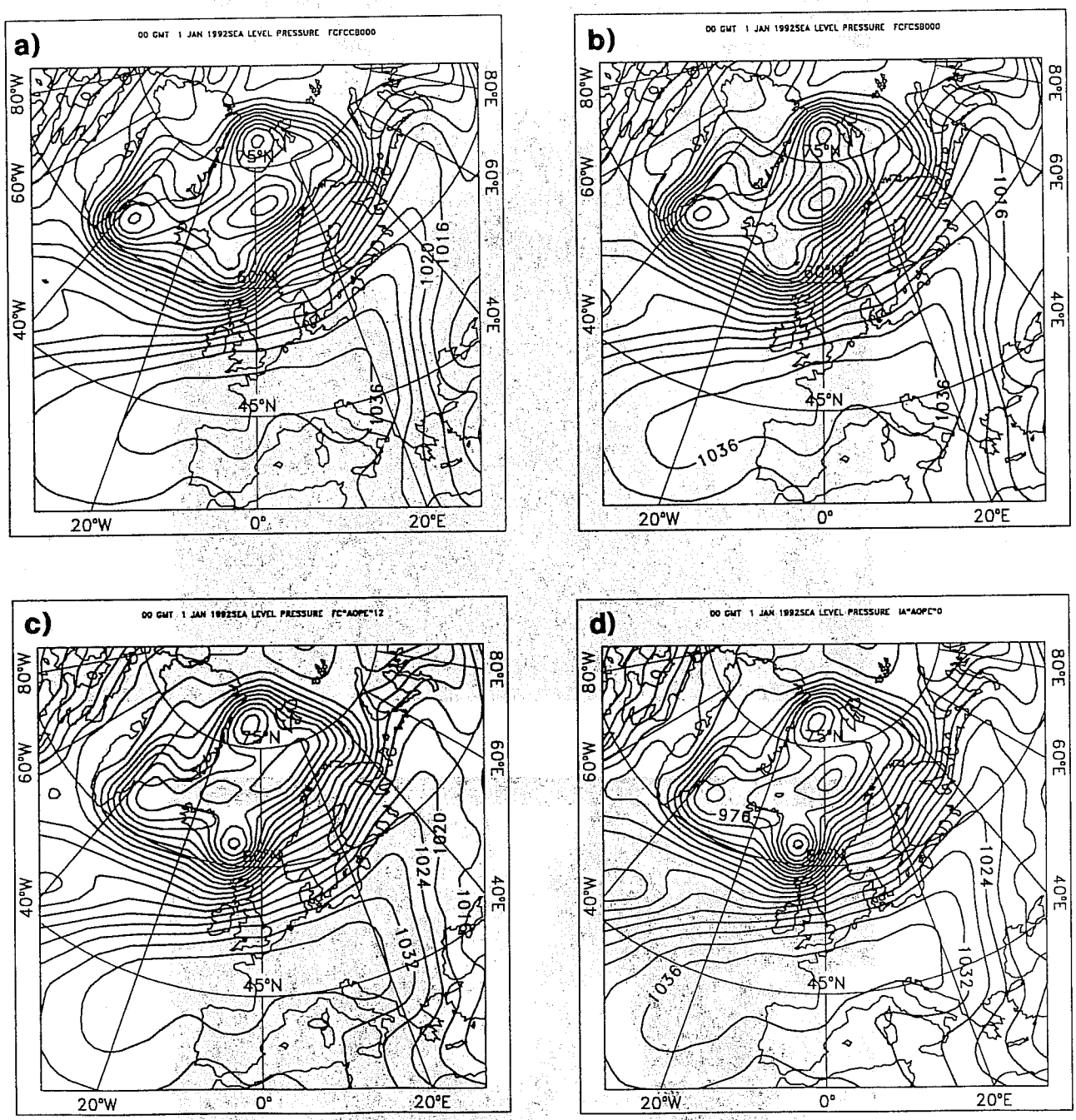

Fig. 14 Mean sea level pressure fields valid 12 UTC 31 December 1991 from (a) the SCATT assimilation, (b) the CONTROL assimilation, (c) the operation forecast and (d) the operational analysis. The forecasts are 12 hour forecasts. Contour interval: 4 hPa.

The SCATT and CONTROL forecasts underestimate the strong storm developing south of Iceland and which is well represented both in the operational forecast and analysis. The lack of physics and the low resolution of the model are certainly detrimental in this case of a small scale rapidly intensifying feature. However, the impact of the σ^0 data persists in the forecast valid 00 UTC. At this time the surface low is nearly cut-off in the SCATT forecast and it is slightly lower in the SCATT than in the CONTROL forecast. These results, although obtained with a crude assimilating model, are quite a bit more encouraging than the forecast results obtained by Hoffman (1993) using the scatterometer winds in the conventional OI assimilation system.

Two further assimilation experiments were run in which conventional surface observations were added to both CONTROL and SCATT. In particular 10 meter wind measurements from ships were included. The impact of the σ^0 data was not significantly changed by the presence of the surface observations.

5 Concluding remarks.

This report describes several 4dVAR data assimilation experiments, which explore the interaction of the model dynamics and the observations when one seeks a solution consistent with both.

In the first examples, of single observations, the resulting analysis increments are proportional to the Kalman filter covariance functions which are implicitly used in 4dVAR. We reconfirm that these covariance functions are flow-dependent (Thépaut et al., 1993), in contrast to those usually specified in OI or 3dVAR assimilation systems. In this case of the exceptional storm of 16 October 87, the baroclinicity of the basic state is reflected in the forecast error covariances.

Similarities between the evolution of the covariances and the evolution of the most unstable modes over the assimilation period is demonstrated. A quantification of this connection might give some *a priori* insight on the spatial structure of the covariances to be used, thereby speeding the minimization process. The connection is however rather indirect. In the first place the covariances are the columns of the matrix RBR^*, while the optimal modes are the eigenvectors of R^*R. Secondly, in some situations the forecast model errors might be significantly larger, negating the assumption of a perfect model necessary for the equivalence of the Kalman filter and the 4dVAR.

As far as the scatterometer data are concerned, encouraging results are obtained despite the crudeness of the assimilating model. These data are able to infer dynamically consistent information in the vertical through the four-dimensional process of the assimilation. There are however, still open scientific questions with regards to several aspects of the definition of J_{scat}:

- A more accurate model function is now available (Stoffelen and Anderson, 1992b).
- The effect of accounting for stability in the boundary layer needs investigation.
- The nonnormality of the distribution of the σ^0 departures might be reduced by using $\ln(\sigma^0)$ in the definition of J_{scat}.

The problem of having a realistic description of the physical processes is a general problem in 4dVAR. Rabier et al. (1992) have shown that a realistic humidity analysis is impossible without condensation processes in the assimilating model. In the present experiments we resorted to using a linearized parametrization of vertical diffusion and surface friction. One solution to the general problem is to develop the adjoint of all physical parametrizations. In that case, we might expect problems of convergence due to highly nonlinear processes in the assimilating model. Instead we plan to approximate the full nondifferentiable minimization problem by a quadratic problem. This strategy, which follows the ideas already under investigation at NMC, is described in detail in Courtier et al. (1992).

6 Acknowledgements.

The collaboration and the support of the ECMWF Research Department Data Assimilation Group is gratefully acknowledged. We thank R. Buizza, A. Stoffelen, A. Persson, M. Hamrud and F. Rabier of ECMWF for helpful discussions and advice. The minimization algorithm was provided by Institut National de Recherche en Informatique et en Automatique (INRIA, France). K.-G. Karlsson from Swedish Meteorological and Hydrological Institute kindly provided us the AVHRR imagery. The work of R. Hoffman was supported by the NASA scatterometer project (Jet Propulsion Laboratory contract 957644, a subcontract to NASA contract NAS7-918). (NASA is the United States National Aeronautics and Space Agency.)

7 References.

Andersson, E., J.-N. Thépaut, J. Eyre, A. McNally, P. Courtier and J. Pailleux, 1992. Use of radiances in 3D/4D variational assimilation. Proc. ECMWF workshop on Variational Assimilation with Emphasis on Three-Dimensional Aspects.

Buizza, R., 1992. Unstable perturbations computed using the adjoint technique. *ECMWF Res. Dep. Technical Memorandum*, **No 189.**

Buizza, R., 1993. Impact of a simple vertical diffusion scheme and on the optimisation time interval on optimal unstable structures. *ECMWF Res. Dep. Technical Memorandum*, **No 192.**

Courtier, P. and O. Talagrand, 1990. Variational assimilation of meteorological observations with the direct and adjoint shallow-water equations. *Tellus*, **42 A**, 531-549.

Courtier, P., C. Freydier, J.F. Geleyn, F. Rabier and M. Rochas, 1991. The Arpege project at Météo-France. Pp 193-232 in Proc. ECMWF seminar on Numerical methods in atmospheric models, 9-13 september.

Courtier, P., J.-N. Thépaut and A. Hollingsworth, 1992. A strategy for operational im-

plementation of 4D-VAR. Proc. ECMWF workshop on Variational Assimilation with Emphasis on Three-Dimensional Aspects.

Daley, R., 1991. Atmospheric Data Analysis. *Cambridge Atmospheric and Space Science Series* (eds Cambridge University Press).

Farrel, B. F., 1989. Optimal excitation of baroclinic waves. *J. Atmos. Sci.*, **46**, 1193-1206.

Francis, R., G. Graf, P. G. Edwards, M. McCaig, C. McCarthy, P. Dubock, A. Lefebvre., B. Pieper, P.-Y. Pouvreau, R. Wall, F. Wechsler, J. Louet and R. Zobl, 1991. The ERS-1 spacecraft and its payload. *ESA bulletin*, **65**, 27-48. ERS-1 Special Issue.

Gauthier, P., 1992. Chaos and quadri-dimensional data assimilation: a study based on the Lorenz model. *Tellus*, **44A**, 2-17.

Gauthier, P., P. Courtier and P. Moll, 1993. Data assimilation with an Extended Kalman-Bucy Filter. To appear *in Mon. Wea. Rev.*.

Gilbert, J. Ch. and C. Lemaréchal, 1989. Some numerical experiments with variable storage quasi-Newton algorithms. *Mathematical Programming*, **B 25**, 407-435.

Heckley, W., P. Courtier, J. Pailleux and E. Andersson, 1992. On the use of background information in the variational analysis at ECMWF. ECMWF workshop on Variational Assimilation with Emphasis on Three-Dimensional Aspects.

Hoffman, R. N., 1993. A preliminary study of the impact of the ERS1 *C*-band scatterometer wind data on the ECMWF global data assimilation system. *Journal of Geophysical Research*, **98**. Accepted for publication.

Hortal, M. and A. J. Simmons, 1991. Use of reduced Gaussian grids in spectral models. *Mon. Wea. Rev.*, **119**, 1057-1074.

Jarraud, M., J. Goas and C. Deyts, 1989. Prediction of an exceptional storm over France and Southern England. *Wea. For.*, **4**, 517-536.

Jazwinski, A. H., 1970. *Stochastic Processes and Filtering Theory.* Academic, New York.

Jones, W. L., L. C. Schroeder, D. H. Boggs, E. M. Bracalente, R. A. Brown, G. J. Dome, W. J. Pierson, and F. J. Wentz., 1982. The SEASAT-A Satellite Scatterometer: The geophysical evaluation of remotely sensed wind vectors over the ocean. *Journal of Geophysical Research*, **87(C5)**, 3297–3317.

Lacarra, J. F., and O. Talagrand, 1988. Short-range evolution of small perturbations in a barotropic model. *Tellus*, **40A**, 81-95.

Long, A. E., 1991. Summary of CMOD2, Wismann, CMOD2-W and CMOD2-1 models. Document Number ESTEC/WMA/AEL/9101, Revision 1, ESTEC, European Spatial Agency.

Lorenc, A.C., 1986. Analysis methods for numerical weather prediction. *Q. J. R. Meteorol. Soc.*, **112**, 1177-1194.

Molteni, F. and T. N. Palmer, 1991. Predictability and finite-time instability of the Northern winter circulation. Pp 101-142 in Proc. ECMWF workshop proceedings on New developments in Predictability.

Pailleux, J., W. Heckley, D. Vasiljevic, J.-N. Thépaut, F. Rabier, C. Cardinali, and E. Andersson. Development of a variational assimilation system. Technical Memorandum 179, ECMWF, Reading, U.K., 1991.

Price, J. C., 1976. The nature of multiple solutions for surface wind speed over the oceans from scatterometer measurements. *Remote Sensing Environ.*, **5**, 47-54.

Rabier, F. and P. Courtier, 1992. Four-dimensional assimilation in the presence of baroclinic instability. *Q. J. R. Meteorol. Soc.*, **118**, 649-672.

Rabier, F., P. Courtier, J. Pailleux, O. Talagrand, J.-N. Thépaut and D. Vasiljevic, 1992. Comparison of four-dimensional variational assimilation with simplified sequential estimation. Proc. ECMWF workshop on Variational Assimilation with Emphasis on Three-Dimensional Aspects.

Schroeder, L. C., D. H. Boggs, G. Dome, I. M. Halberstam, W. L. Jones, W. J. Pierson, and F. J. Wentz, 1982. The relationship between wind vector and normalized radar cross section used to derive SEASAT-A satellite scatterometer winds. *Journal of Geophysical Research*, **87(C5)**, 3318–3336.

Schultz., H., 1991. A circular median filter approach for resolving directional ambiguities in wind fields retrieved from spaceborne scatterometer data. *Journal of Geophysical Research*, **95(C4)**, 5291–5304. Errata in number **C6**, page 9783.

Simmons, A. and D.Burridge, 1981. An energy and angular momentum conserving vertical finite difference scheme and hybrid vertical coordinate.*Mon. Wea.Rev.*, **109**, 758-766

Simon, H. D., 1984. The Lanczos algorithm with partial re-orthogonalization. *Math. Comp.*, **42, 165**, 115-142

Shaw D., P. Lonnberg, A. Hollingsworth and P. Unden, 1987. Data assimilation: The 1984/85 revisions of the ECMWF mass and wind analysis.*Q. J. R. Meteorol. Soc.*, **113**, 533-566.

Stoffelen, A. and D. L. T. Anderson, 1992a. ERS-1 scatterometer calibration and validation activities at ECMWF: A. The quality and characteristics of the radar backscatter measurements. In *European "International Space Year" Conference.*, Munich, Germany, 30 March - 5 April.

Stoffelen, A. and D. L. T. Anderson, 1992b. ERS-1 scatterometer data characteristics

and wind retrieval skill. In *First ERS-1 Workshop*, Cannes, France, 4 - 6 November. To be published by European Space Agency.

Thépaut J.-N., and P. Courtier, 1991. Four-dimensional variational data assimilation using the adjoint of a multilevel primitive-equation model. *Q. J. R. Meteorol. Soc.*, **117**, 1225-1254.

Thépaut J.-N., D. Vasiljevic, P. Courtier and J. Pailleux, 1993. Variational assimilation of conventional meteorological observations with a multilevel primitive equation model. *Q. J. R. Meteorol. Soc.*, **119**, 153-186.

Undén., P., 1989. Tropical data assimilation and analysis of divergence. *Monthly Weather Review*, **117**, 2495-2517.

Vasiljevic, D., C. Cardinali and P. Unden, 1992. ECMWF 3D variational data assimilation of conventional observations. Proc. ECMWF workshop on Variational Assimilation with Emphasis on Three-Dimensional Aspects.